Liquid Crystals
Publication details, including instructions for authors and subscription information:
http://www.informaworld.com/smpp/title~content=t713926090

The role of surface tilt in the operation of pi-cell liquid crystal devices

E. J. Acosta[a]; M. J. Towler[a]; H. G. Walton[a]
[a] Sharp Laboratories of Europe Ltd, Edmund Halley Road, Oxford Science Park, Oxford OX4 4GB, UK,

Online publication date: 06 August 2010

To cite this Article Acosta, E. J. , Towler, M. J. and Walton, H. G.(2000) 'The role of surface tilt in the operation of pi-cell liquid crystal devices', Liquid Crystals, 27: 7, 977 — 984
To link to this Article: DOI: 10.1080/02678290050043932
URL: http://dx.doi.org/10.1080/02678290050043932

LIQUID CRYSTALS, 2000, VOL. 27, NO. 7, 977–984

The role of surface tilt in the operation of pi-cell liquid crystal devices

E. J. ACOSTA*, M. J. TOWLER and H. G. WALTON

Sharp Laboratories of Europe Ltd, Edmund Halley Road, Oxford Science Park, Oxford OX4 4GB, UK

(*Received 19 November 1999; accepted 24 January 2000*)

The role of surface tilt in the operation of pi-cells (OCB) is discussed. We show the effect of tilt on the relative stability of the H and V states, the switching characteristics and the domain growth speed. We further study the effects of temperature and cell thickness on the domain growth.

1. Introduction

The pi-cell [1, 2] or optically compensated bend mode (OCB) [3] is a fast electro-optic response speed device, in which the voltage-induced optical change occurs primarily by reorientation of the director near the boundary substrates. It has recently gained renewed device interest as a fast mode for improved video display performance [4]. The device consists of a nematic confined by parallel alignment of typically 2°–5° tilt. At zero applied voltage these conditions stabilize a splayed director configuration, or H state (H_S). On applying a field, alternative director configurations become energetically favourable over the H state. There are four director configurations that are important in the operation of a pi-cell: the symmetric H state (H_S), the asymmetric H state (H_A), the 180° twist state (T state) and the bend state (V state), these are depicted in figure 1.

If no voltage is applied the symmetric H state (H_S) is stable. Applying a voltage greater than the stability voltage (V_{st}) favours the V state. As the H state is topologically distinct from the V state, the transition from one to the other requires the generation of an $S = \pm 1/2$ disclination to nucleate the favoured state [5]. This discontinuous transition (process of nucleation and growth) takes some time to occur, during which the H_S state may undergo a Fréedericksz transition into the asymmetric splayed state (H_A). Similarly, starting at a high voltage in a stable V state and reducing the voltage below V_{st} permits the nucleation of the H state, again; this discontinuous transition takes a finite time, during which the V state can undergo a second order phase transition into the 180° twist state (T state).

*Author for correspondence; e-mail: zabbie@sharp.co.uk

The fast electro-optic response speeds of the pi-cell are obtained by utilizing the V state as the operating state, as shown in figure 1. The pi-cell is positioned between crossed polarizers, with the alignment direction at 45° to their polarization axes. To cancel the residual LC retardation and obtain a dark state at a finite voltage, a retarder is placed between the pi-cell and one of the polarizers. Typically the cell gap, birefringence and retarder are chosen to operate the device between approximately 2 and 5 V, switching between a net $\lambda/2$ and 0 retardation.

2. The stability of states

2.1. *H and V stability at zero applied field*

A tractable analytic expression relating to the threshold voltage for the H–V transition has not been found. Generally, numerical solutions to the full Euler–Lagrange equations must be determined. However, considerable simplification of the equations is possible when determining the tilt (θ_p) required to stabilize a (untwisted) V state with respect to the H state at zero applied field

The free energy per unit area F for an untwisted nematic in one dimension is given by:.

$$F = \frac{1}{2}\int_0^d (K_{11}\cos^2\theta + K_{33}\sin^2\theta)\left(\frac{\mathrm{d}\theta}{\mathrm{d}z}\right)^2 \mathrm{d}z \qquad (1)$$

where θ = tilt angle of the director and $\theta = 0°$ is in the plane of the cell surfaces, K_{11} = splay elastic constant, K_{33} = bend elastic constant and d = cell thickness. Writing the Euler–Lagrange equation, multiplying by $\theta_z/2$ and

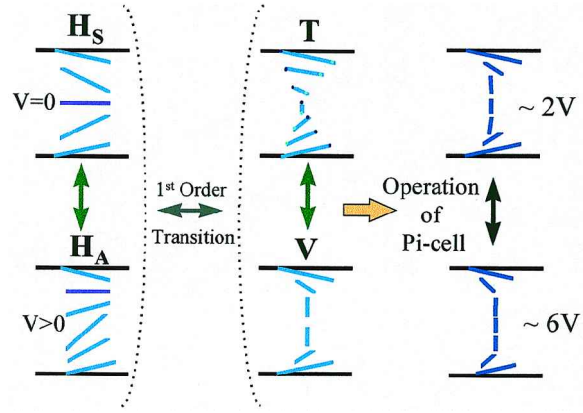

Figure 1. Director configurations within a pi-cell.

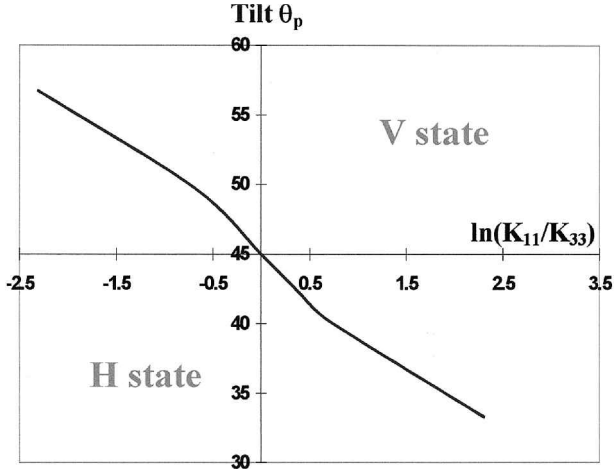

Figure 2. Relative stability of the H and V states at a given pretilt θ_p calculated as a function of the elastic constants $\ln(K_{11}/K_{33})$ at zero applied field.

integrating once gives:

$$(K_{11}\cos^2\theta + K_{33}\sin^2\theta)\left(\frac{d\theta}{dz}\right)^2 = \text{const} \qquad (2)$$

whence,

$$\frac{d\theta}{dz} = \pm\left(\frac{\text{constant}}{K_{11}\cos^2\theta + K_{33}\sin^2\theta}\right)^{1/2} \qquad (3)$$

substituting back into the free energy yields:

$$F = \int_0^d \text{const}\ dz. \qquad (4)$$

This expression applies to an arbitrary untwisted nematic in one dimension and states that in equilibrium and for zero applied field the free energy density is independent of z. This is physically clear, since an excess of elastic energy density at some point would cause the system to move to reduce this energy gradient, i.e. equilibrium would not have been attained.

For the H state and V state to have equal energy, the constant in equation (4) must be the same for both, hence integrating from $z = 0$ (where $\theta = \theta_p$) to the centre of the cell for both states gives:

$$\int_{\theta=\theta_p}^{\theta=\pi/2} (K_{11}\cos^2\theta + K_{33}\sin^2\theta)^{1/2}\,d\theta + \int_{\theta=\theta_p}^{\theta=0} (K_{11}\cos^2\theta + K_{33}\sin^2\theta)^{1/2}\,d\theta = 0 \qquad (5)$$

where we have been careful to choose the correct sign of the gradient $d\theta/dz$ in each case. Equation (5) is trivially solved numerically to find the tilt θ_p (for a given K_{11} and K_{33}) which stabilizes the V state with respect

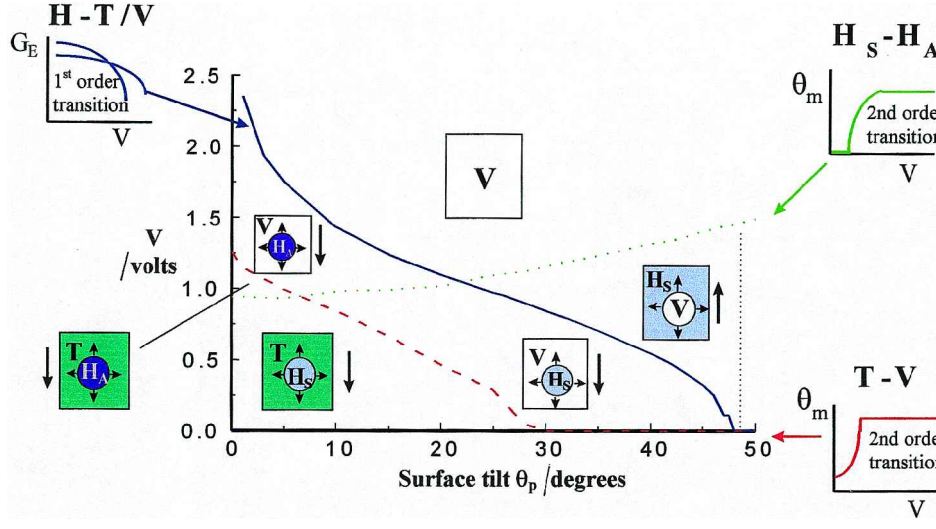

Figure 3. Relative stability of the states in a pi-cell as a function of surface tilt. Arrows denote whether diagrammatic representation of the domains occurs on increase (↑) or decrease (↓) of voltage.

to the H state; figure 2 shows this result. As expected, for $K_{11} = K_{33}$, the H and V states require a surface tilt of 45° to be stable at zero field.

2.2. *Symmetric and asymmetric surface tilts.*

Introducing an asymmetry between the top and bottom surface tilts in a pi-cell will alter the stability of states at zero field from that described in figure 2. In the case of highly asymmetric surface tilts, e.g. very high surface tilt on one substrate and very low surface tilt on the other, an H–V transition is not exhibited. We do not consider the case of asymmetric surface tilts in detail.

2.3. *Finite field, H_S, H_A, V and T stability*

The relative stability of the states within a driven symmetric surface tilt pi-cell is calculated [6] for a 5 μm cell of nematic liquid crystal E7 (Merck Ltd. UK) at 25°C ($\Delta\varepsilon = 13.745$, $K_{11} = 10.643$ pN, $K_{22} = 6.7$ pN, $K_{33} = 15.5$ pN). In this calculation, the nucleation process need not be considered as the stabilities of the states relate to the system in equilibrium.

The stability voltage (V_{st}) at various surface tilts (θ_p) were determined by locating the voltage at which the Gibbs free energy (G) of the H state equalled that of the V state ($\Delta G = 0$), and is represented by the solid line in figure 3. The mid-plane tilt of the director (θ_m) for both the H and V states was calculated as a function of voltage for various surface tilts to determine at which voltages the second order transitions occur: the $H_A \leftrightarrow H_S$ transition corresponds to the dotted line in figure 3 and the T↔V transition to the dashed line in figure 3. Experimentally, at the stability voltage (V_{st}) one would observe the velocity of the $S = \pm 1/2$ disclination line between the H and V states to be zero, while the asymmetric H_A state can be observed in the form of tilt walls on application of suitable voltages to symmetric tilt cells.

The interaction between the states (for this specific pi-cell) is summarized in figure 3 as a function of the surface tilt. Good agreement was observed between the calculated results and experimental observations:

(1) The stability voltage decreases as tilt increases.
(2) The V state is stable at all voltages for surface tilts above ~48°, eliminating the need for nucleation. Xu, *et al.* [7] show this experimentally for surface tilts of 51°.
(3) The twist state does not appear at surface tilts above ~30°.

A brief investigation of the elastic and electrostatic energies of the system indicated that it is the combined effect of the energies that govern the H–V transition; neither dominates.

3. Switching characteristics of the pi-cell at low and high surface tilts

3.1. *Transmission–voltage characteristic*

To investigate the effect of surface tilt on the operation of the pi-cell, the electro-optic curves of low and high tilt pi-cells were measured (without additional retardation films) see figure 4. Increasing the surface tilt decreased the voltage ($V_{T\text{-max}}$) at which the maximum transmission occurred. The reduction of $V_{T\text{-max}}$ permits a reduction in the operating voltage of the pi-cell, as sufficient optical modulation is still present for operation (so long as $V_{T\text{-max}}$ remains greater than the stability voltage, recalling that the stability voltage decreases as tilt increases). However, at very high tilts, approximately greater than 55°, the optical modulation becomes very much reduced.

3.2. *Relaxation times*

Relaxation times were measured to determine the effect of surface tilt. Measurements were made in 5.2 μm thick cells filled with E7, for a range of tilts (3.2°, 16.5°,

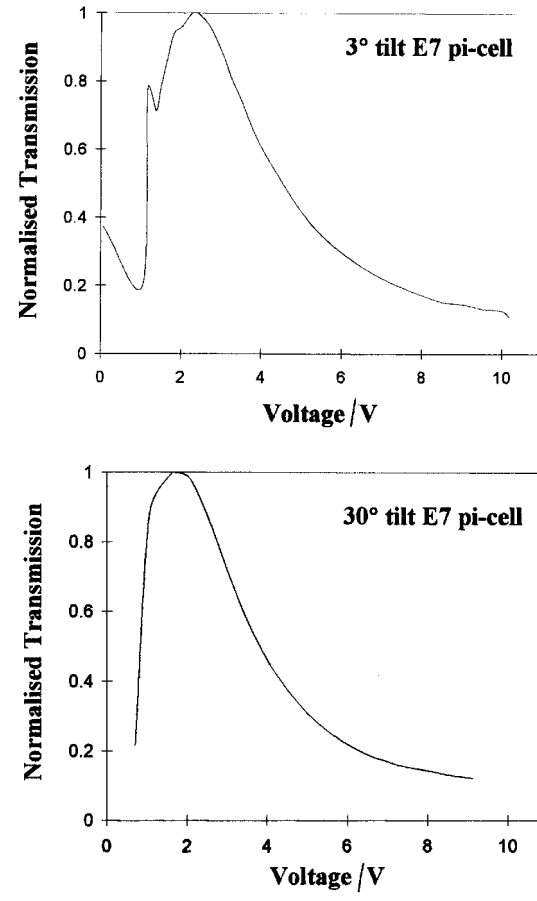

Figure 4. Normalized transmission–voltage curve for low and high tilt pi-cells (5 μm, E7 cells at 45° to crossed polarizers and no retarder).

17°, 20°, 30° and 32°). The relaxation times for a pi-cell (with no additional retarders) were obtained by first determining the voltages at which maximum transmission occurs in the respective cells. The relaxation times correspond to the time taken to relax from 10% to 90% of the maximum transmission when switched from 10 V (arbitrarily chosen) to the respective voltage of maximum transmission. When crossing the pi-cell with a 52 nm retarder, the voltages at which minimum and maximum transmissions occur had to be determined. The relaxation times correspond to the time taken to relax from 10% to 90% of the maximum transmission when switched between the respective minimum and maximum transmission voltages. The results are plotted in figure 5. The ON-times of the cells varied, but remained under 1 ms.

Interestingly, very little difference is seen in the relaxation times for tilts below 20°—an increase from 1.8 to 2.3 ms (no additional retarder) and from 2.4 to 3.4 ms when a 52 nm retarder was incorporated into the set-up. However, for tilts greater than 20° there is a marked increase in the relaxation time, reaching 4.7 ms in pi-cells of 32° tilt (no retarder), nearly twice that of the 3° tilt cell. This suggests that the pi-cell can be operated with tilts of up to approximately 20° without a detrimental effect on the switching performance. However a more detailed study would be required for particular display requirements, the definition of relaxation time (e.g. 10%–90% compared with 5%–95% transmission) obviously affecting that which is measured.

4. Domain wall between H and V states

The effect of the surface tilt on the behaviour of the domain wall between the two states was investigated by measuring the speed of the disclination line between the H and V domains as a function of the voltage applied.

4.1. *Theory*

For large domains we assume (dimensionally):

$$\underset{\text{Pa s}}{\text{Effective viscosity } (\eta)} \times \underset{\text{m s}^{-1}}{\text{Wall speed } (s)} \approx \underset{\text{J m}^{-2}}{\text{Excess free energy density } (\Delta G)} \tag{6}$$

The excess Gibbs free energy per unit area is obtained by calculating the difference between the Gibbs free energy density of the H state and the V (or T) state. We first calculate the difference between the H and V state configuration (figure 6) assuming isotropic elastic constants (K), under large uniform electric fields (E).

For each case:

$$\text{energy per unit area} = \frac{1}{2}\int_0^\infty (K\theta_z^2 - \varepsilon_0 \Delta\varepsilon E^2 \sin^2\theta)\,\mathrm{d}z \tag{7}$$

where $\Delta\varepsilon$ is the dielectric anisotropy. Let

$$\xi = \left(\frac{K}{\varepsilon_0 \Delta\varepsilon}\right)^{1/2} \frac{1}{E}; \quad Z = \frac{z}{\xi}$$

giving:

$$\text{energy per unit area} = \frac{E(K\varepsilon_0\Delta\varepsilon)^{1/2}}{2}\int_0^\infty (\theta_z^2 - \sin^2\theta)\,\mathrm{d}Z \tag{8}$$

leading to:

$$\Delta G \text{ per unit area} = \frac{2V}{d}(K\varepsilon_0\Delta\varepsilon)^{1/2}\sin\theta_\mathrm{P}. \tag{9}$$

The domain growth (V replacing H) speed at high voltages is expected to be inversely proportional to the cell thickness d and proportional to the surface tilt angle θ_P, the voltage V and an effective viscosity η.

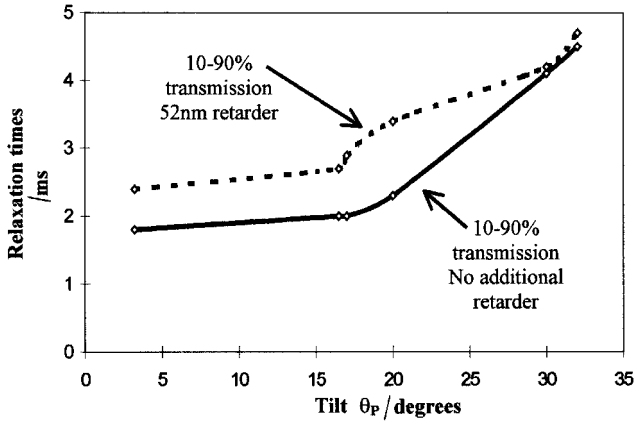

Figure 5. Relaxation times for different tilt pi-cells.

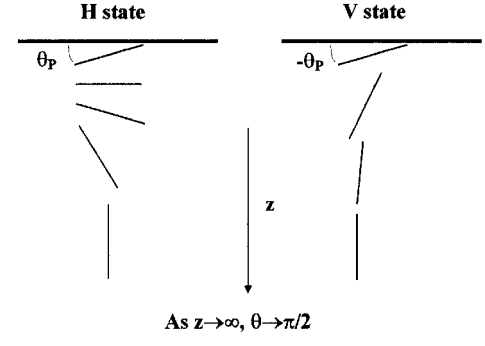

Figure 6. Schematic representation of the difference between the H and V states as used to determine the analytical expression for the excess Gibbs free energy.

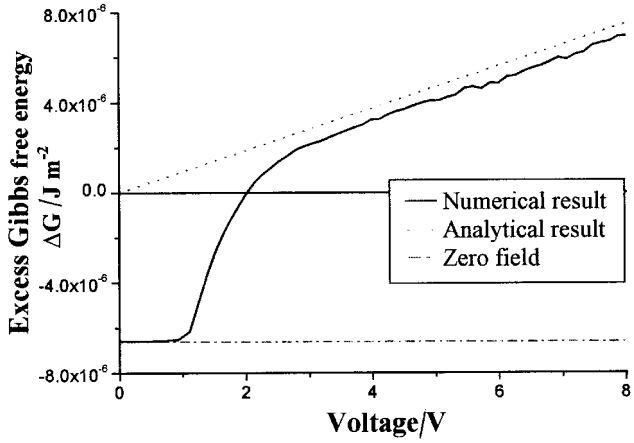

Figure 7. Numerical (solid line) and analytical (dotted lines) determination of the excess Gibbs free energy (ΔG) for a 2° tilt E7 pi-cell.

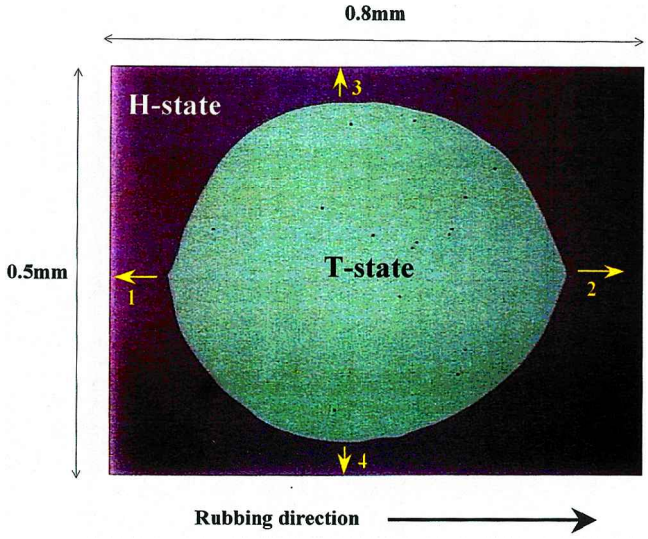

Figure 8. Microphotograph of a V state (grey) domain relaxed to a T state within an H state (purple) at zero applied field. Labelled 1–4 are the four points along the domain wall at which the domain speed is measured.

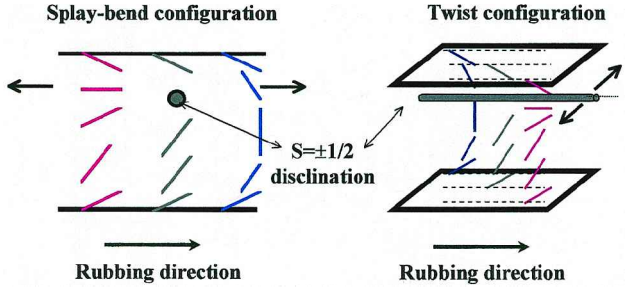

Figure 9. Schematic representation of the splay–bend and twist wall director configurations about the $S = \pm 1/2$ disclination along the domain wall. Arrows (→) indicate direction of wall movement.

Additionally, the domain growth (H replacing T) at low voltages and low surface tilt is expected to be independent of voltage (K_2 twist elastic constant) with:

$$\Delta G \text{ per unit area} = \frac{K_2 \pi^2}{2d}. \qquad (10)$$

In practice, the excess Gibbs free energy density is calculated numerically. Such a calculation for E7 ($K_1 = 10.643$ pN, $K_2 = 6.7$ pN, $K_3 = 15.5$ pN, $\Delta\varepsilon = 13.745$, $d = 5\,\mu$m) is represented by the solid line in figure 7. The predictions obtained from the simple analytic theory

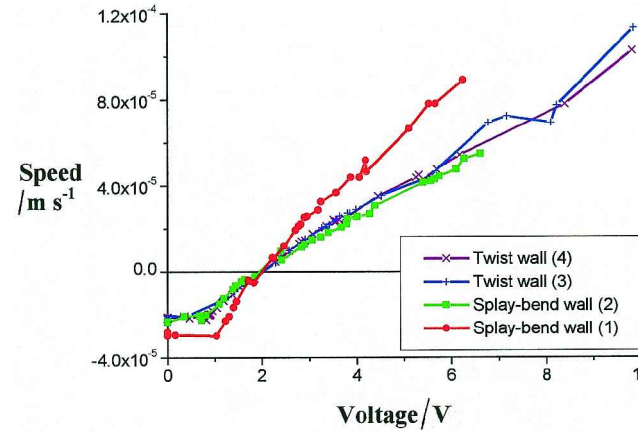

Figure 10. Domain wall speeds measured as a function of voltage in a 5 µm, 11.5° tilt E7 cell.

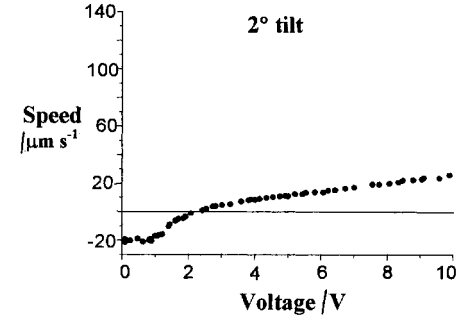

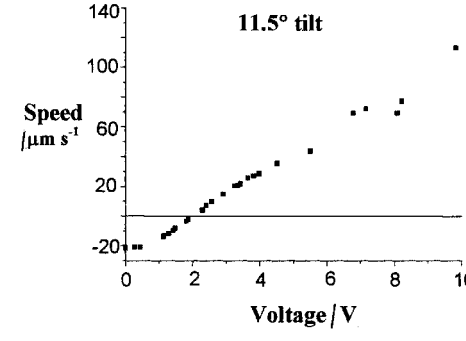

Figure 11. Speed of the twist-wall as a function of voltage in a 2° and an 11.5° tilt, 5 µm E7 pi-cells.

with equation (9) multiplied by $(\varepsilon_{\parallel}/\varepsilon_{\perp})^{1/2}$ to allow for the non-uniform E-field and taking $K = K_1$, represented by the dotted line in figure 7, are however a reasonable approximation.

4.2. *Experiment*

The microphotograph in figure 8 shows a T state domain within an H state in a pi-cell at zero field (decreasing T state domain). In the experiment the V (and T) state domain must be of the order of millimetres to ensure that the domain size does not affect the speed of the domain wall. The domain speed was measured as a function of voltage at four locations, labelled 1–4 in figure 8, corresponding to two splay–bend configurations (types 1, 2); a portion of the domain wall moving parallel to the alignment direction and two twist configurations (types 3, 4); domain wall motion orthogonal to the alignment direction. Figure 9 illustrates the respective director configurations about the splay–bend and the twist disclination lines.

4.3. *Asymmetric domain growth speed*

The domain growth along the four directions labelled (1, 2, 3, 4) in figure 8 were investigated. The speed of the two splay–bend (1, 2) and two twist (3, 4) walls were measured in cells of different tilt (2°, 11.5°, 15°) and thickness (2.3, 5, 10.5 μm). Figure 10 shows the wall speeds measured in an (5 μm, 11.5°) E7 cell. It was observed that the domain speed for the splay–bend wall (type 1) was significantly faster than the other three (types 2, 3, 4) domain wall speeds regarding both growth and shrinkage. This behaviour was observed in all the cells measured though it was less marked at lower tilts. This asymmetry in the speed of the domain wall is probably the result of the net flow effect in a pi-cell upon applying/removing a field.

4.4. *Effect of surface tilt on the domain speed*

Graphs showing the speed of the twist wall as a function of voltage in 2° and 11.5° tilt (5 μm) E7 pi-cells

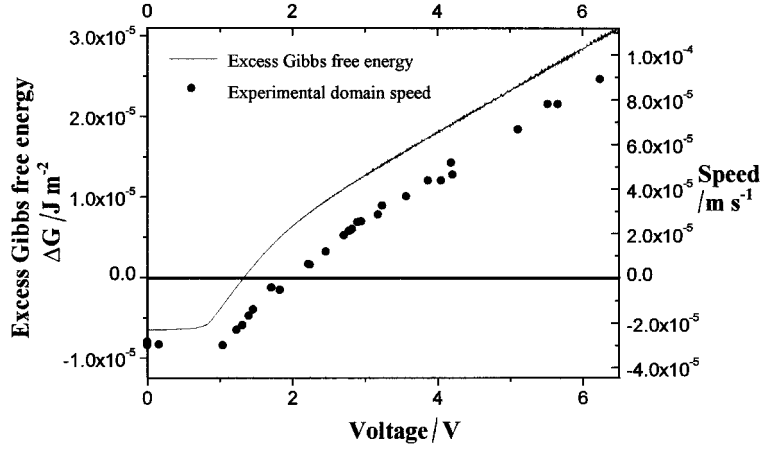

Figure 12. Fitting the experimental domain speed data for a 11.5° tilt pi-cell to the numerical excess Gibbs free energy (ΔG) data to determine an effective viscosity (η) results in $\eta = 0.277$.

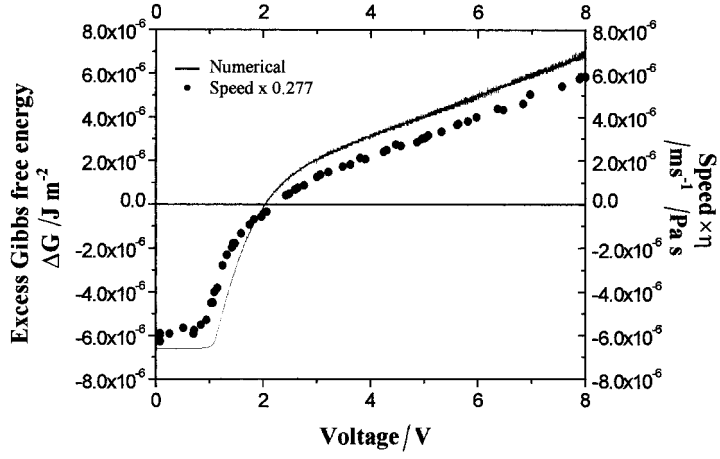

Figure 13. Comparison of the measured (●) splay–bend wall speed in a 2° tilt pi-cell, multiplied by the effective viscosity ($\eta = 0.277$ Pa s), with the numerical excess Gibbs free energy (−) calculated for an equivalent cell.

are shown in figure 11. These graphs support equations (9) and (10):

(1) At high voltages the speed of the domain is proportional to the voltage applied.
(2) At high voltages, the domain speed increases with the surface tilt, e.g. domain speed at 10 V is 26 μm s^{-1} at 2° tilt and 118 μm s^{-1} at 11.5° tilt.
(3) The shape of the curve at low voltages is dictated by the surface tilt of the pi-cell and the low tilt graph agrees with the shape of the curve in figure 7.

It was observed that the difference in domain speed between the splay–bend wall (1) and the other three domain walls increased with surface tilt, such that at low tilts (2°) there was approximately a 20% difference between them, while at higher tilts (15°) there was approximately a 50% difference. The effective viscosity can be determined from expression (6), by comparing the experimental domain speeds with the calculated excess Gibbs free energy plots. Figure 12 compares the experimental domain speed for a splay–bend wall (type 1), direction of growth against the rubbing direction, in a 5 μm, 11.5° tilt pi-cell with the numerically calculated excess Gibbs free energy for an equivalent pi-cell. Comparing the gradient of the two curves at high voltages gives an effective viscosity, η; from figure 12 $\eta = 0.277$ Pa s.

Repeating the procedure for a twist wall results in an effective viscosity of 0.458 Pa s. Although this value is significantly greater than the value of 0.277 Pa s, both effective viscosity values are of the order of the rotational viscosity of E7, $\gamma_1 = 0.399$ Pa s. To verify the validity of the effective viscosity ($\eta = 0.277$ Pa s, was calculated for a relatively high tilt pi-cell), the splay-bend (1) domain speed measured in a low tilt (2°) pi-cell was scaled by $\eta = 0.277$ Pa s. A comparison with the calculated excess Gibbs free energy, figure 13, shows reasonable agreement.

4.5. *Cell thickness*

The effect of cell thickness was investigated for 11.5° tilt pi-cells. The measured domain wall speed in 2.3, 5 and 10.5 μm thick cells along all the four directions described in figure 8 are shown in figure 14. It was observed that at high and low voltages, away from the stability voltage, the speed of the domain growth (shrinkage) scaled as $1/d$. This behaviour held true for all four measured locations about the domain wall even though the speed of the splay–bend wall (1) exhibits a different speed from the others. The stability voltage, for similar sized domains was observed to decrease as the cell thickness increased. This is not explained by a simple one dimensional energy comparison between the two states: a calculation for the equivalent E7 pi-cell gave a (thickness independent) stability voltage of $V_{st} = 1.33$ V. The calculated stability voltage is significantly less than that measured: $V_{st} \sim 2.3$ V for a 2.3 μm and $V_{st} \sim 2.0$ V for a 5 μm pi-cell. Increasing the thickness of the cell reduces the measured V_{st} towards the theoretical value, indicating that the domain wall energy does not scale with similar thickness dependence as the domains; this remains to be investigated.

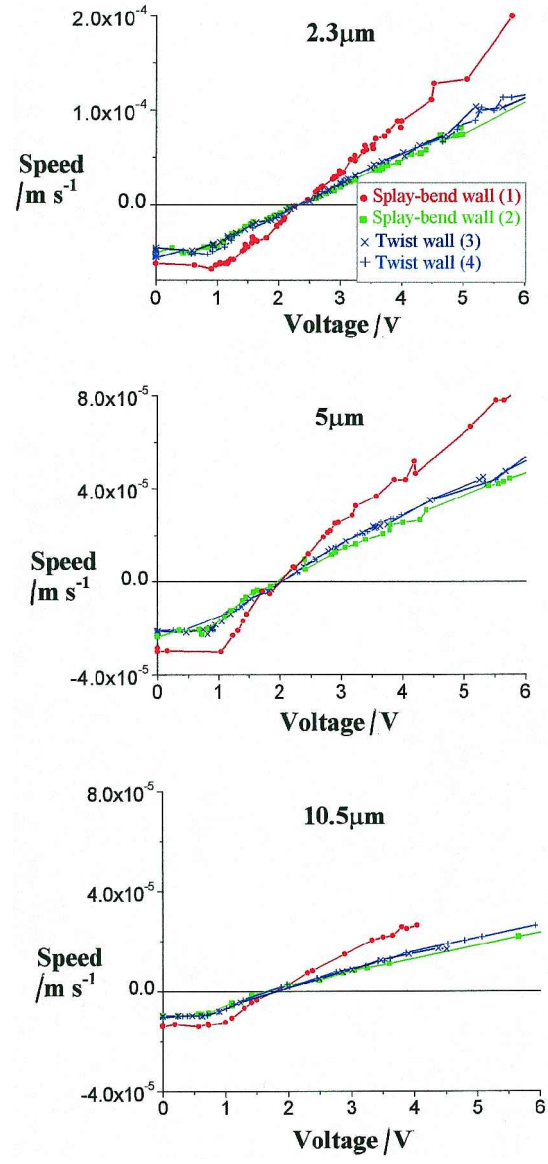

Figure 14. Domain wall speeds measured for different thickness pi-cells (11.5° tilt).

4.6. *Temperature*

While the bulk of the investigation was done using E7 as the nematic LC, in a pi-cell device a TFT compatible nematic LC would have to be employed. For this reason we chose to investigate the effect of temperature in

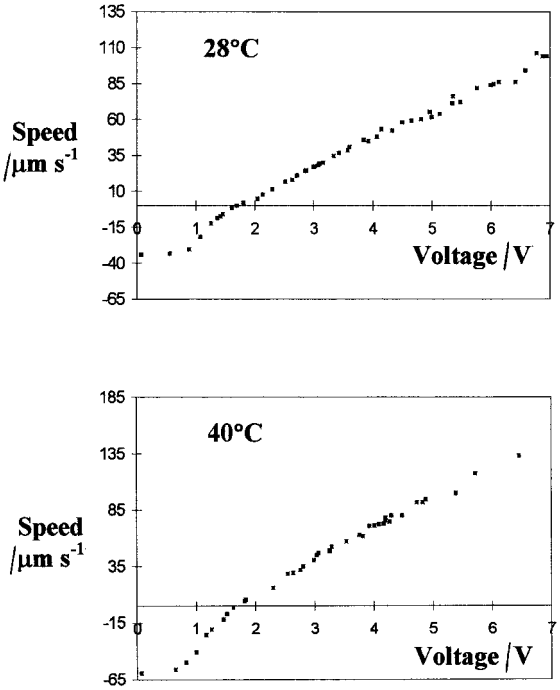

Figure 15. Twist-wall domain speed measured as a function of voltage at different temperatures.

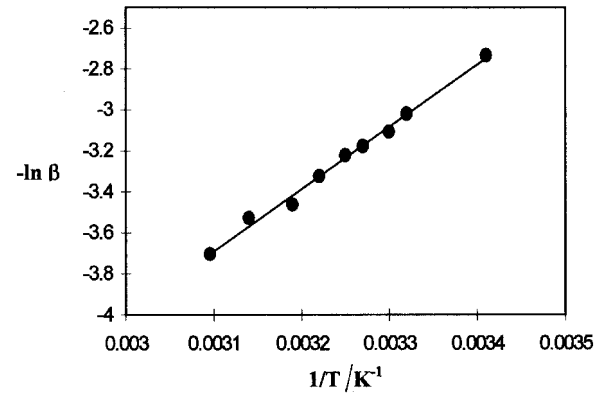

Figure 16. Domain wall speed as a function of temperature.

5 μm (~14° tilt) pi-cells filled with MLC-6000-100, a low level multiplexing LC (Merck); $\Delta\varepsilon = 10.4$, $K_{11} \sim 12.5$ pN, $K_{22} \sim 7.3$ pN, $K_{33} \sim 17.9$ pN (at 20°C). The speed of the twist wall was measured at temperatures ranging from 20 to 50°C. Two of the resulting graphs appear in figure 15. The stability voltages in these cells varied only very slightly over the temperature range measured: $V_{st} = 1.70$ V at 28°C compared with $V_{st} = 1.63$ V at 40°C. However the stability voltage for other LC materials has been observed to increase with temperature (MLC 13300-100, Merck) while decreasing in others (E7, Merck).

The gradient (β) of the domain speed–voltage curve for voltages greater than V_{st}, was calculated and found to increase with temperature. We expect the behaviour of the domain wall speed to be proportional to the effective viscosity (η), with temperature behaviour:

$$\eta = k \exp\left(\frac{\xi}{T}\right) \tag{11}$$

where k = constant, ξ = activation energy, T = temperature in Kelvin, and $\eta \propto 1/\beta$.

Taking the logarithm:

$$-\ln(\beta) \sim \ln k + \left(\frac{\xi}{T}\right). \tag{12}$$

Plotting the logarithm of the measured gradients (β) against T^{-1} results in a linear behaviour as shown in figure 16 which indicates that these results are in agreement with the Arrhenius behaviour.

5. Conclusions

This work has clarified the role of pretilt in the stability of the states occurring in a pi-cell. As previously suggested [7], tilt of the order of 45° can stabilize the V state at zero volts, but this is at the cost of switching speed and optical modulation. Away from the stability voltage the speed of growth of the domains is that expected from a simple difference in the Gibbs energy density of the two states.

Asymmetry in domain growth speed is thought to be due to the coupling with flow, and this requires further investigation. Finally the nature of the domain wall and its role in voltage stability and effective viscosity require clarification.

References

[1] Berezin, P. D., Blinov, L. M., Kompanets, I. N., and Nikitin, V. V., 1973, *Sov. J. quant. Electron*, **3,** 78.
[2] Bos, P. J., and Koehler/Beran, K. R, 1984, *Mol. Cryst. liq. Cryst.*, **133,** 329.
[3] Miyashita, T., Vetter, P., Suzuki, M., Yamaguchi, Y., and Uchida, T., 1993, In Proceedings of Conference Eurodisplay '93, LCT-6, 149.
[4] Noguchi, M., and Nakamura, H., 1997, *SID 97 Dig.*, P-61, 839.
[5] Cheng, J., 1981, *J. appl. Phys.*, **52,** 724.
[6] Software modelling package 1Dimos, autronic-melchers@t-onlinede
[7] Xu, M., Yang, D-K., Bos, P. J., Jin, X., Harris, F. W., and Cheng, S. Z. D., 1998, *SID 98 Dig.*, 11.4L, 139.